International Journal of Surface Science and Engineering

ISSN online: 1749-7868 - ISSN print: 1749-785X
https://www.inderscience.com/ijsurfse

Effect of impingement angle and impact velocity on slurry erosive wear behaviour of particulate reinforced aluminium composites

S. Annamalai, B. Anand Ronald, D. Ebenezer

DOI: 10.1504/IJSURFSE.2023.10058586

Article History:

Received:	29 March 2023
Last revised:	25 May 2023
Accepted:	13 June 2023
Published online:	15 February 2024

Effect of impingement angle and impact velocity on slurry erosive wear behaviour of particulate reinforced aluminium composites

S. Annamalai*, B. Anand Ronald and D. Ebenezer

Department of Mechanical Engineering,
Sri Sivasubramaniya Nadar College of Engineering,
Chennai, Tamil Nadu, India
Email: annamalaisv95@gmail.com
Email: anandronald@rediffmail.com
Email: ebenezerd@ssn.edu.in
*Corresponding author

Abstract: The influence of impact velocity (10, 20, and 30 m/s) and impact angle (45°, 60°, 75°, and 90°) on the slurry erosive wear behaviour of SiC-reinforced Al 2124 matrix composite was determined. The composite was synthesised by powder metallurgy route and the optical microscopic image confirmed the uniform distribution of SiC particles in the Al 2124 matrix. The microstructural analysis of the eroded surfaces showed that micro-cutting, ploughing, craters, and particle pull-out were the primary material removal mechanisms. The mass loss was observed to increase by increasing the impact velocity and the maximum mass loss was reported at 45°–60° impact angles with 30 m/s impact velocity. The XRD analysis revealed that there was no quartz inclusion on the eroded surface. The inconsistent microhardness values resulted because of the exposed SiC particles on the surface and the crater formation. The variation in average roughness significantly increased by increasing the flow velocity.

Keywords: slurry erosion; metal matrix composite; erosion wear; erodent; impingement angle.

Reference to this paper should be made as follows: Annamalai, S., Ronald, B.A. and Ebenezer, D. (2024) ‘Effect of impingement angle and impact velocity on slurry erosive wear behaviour of particulate reinforced aluminium composites’, *Int. J. Surface Science and Engineering*, Vol. 18, No. 1, pp.1–21.

Biographical notes: S. Annamalai is a PhD student at Sri Sivasubramaniya Nadar College of Engineering (registered under Anna University), Chennai, Tamilnadu, India. He graduated from Mechanical Engineering at Loyola-ICAM College of Engineering and Technology, Chennai, India. He received his ME from Alagappa Chettiar Government College of Engineering and Technology, Karaikudi, India in 2018. His research topic focuses on the slurry erosion of stainless steel and metal matrix composites (MMCs).

B. Anand Ronald is working as an Associate Professor at the Department of Mechanical Engineering, Sri Sivasubramaniya Nadar College of Engineering, Chennai. He received his BE degree in Mechanical Engineering at Bharathiyar university in 1999 and his ME in Production Engineering from Annamalai

University in 2002. He did his PhD at the Indian Institute of Technology, Madras. He has published more than 20 research papers in various international journals. His research area includes MMCs, tribology, metal casting, machining of advanced materials, and friction stir processing.

D. Ebenezer is an Assistant Professor at the Department of Mechanical Engineering, Sri Sivasubramaniya Nadar College of Engineering, Chennai. He did his BE in Mechanical Engineering at the University of Madras. He received his ME in Energy engineering degree from PSG College of Technology, Coimbatore in 2003. He received his PhD from Anna University, Chennai in 2022. His works are about diffusion bonding, impression creep thermal systems, energy conversion, and solar systems.

1 Introduction

Erosion is a type of mechanical wear that often affects engineering components. Erosion occurs by the impingement of hard solid erodents on the target surface with high kinetic energy imparted by the working medium, either air or liquid. The material loss or wear significantly reduces the service life of the components. It has been posed as a serious issue in many applications that handle particle-entrained mediums (Yadav et al., 2022). The mechanism of erosion varies concerning the nature of the material. For instance, upon impingement of an erodent particle, in ductile material, material loss occurs by the plastic deformation and subsequent impingements remove the material from the target material in the form of chips. Fracturing was observed in the brittle material when the erodent impacted it. Material erosion is influenced by many parameters like target material properties, erodent properties, flow characteristics, and slurry properties (Miyazaki and Funakura, 1996; Ishfaq Amin and Harmain, 2021).

Composites are a novel category of materials formed by mixing two materials, namely metal, ceramic, and polymer. Metal matrix composites (MMCs) have been used instead of metallic materials owing to their improved mechanical properties that can withstand severe working conditions. Aluminium, magnesium, and titanium are often used as matrix materials because of their lightweight and corrosion-resistance properties. For instance, hard and stiff ceramic particles are added to the soft matrix material to obtain the MMCs with tailor-made properties (Aribo et al., 2017). Furthermore, the properties of composites are enhanced by adding reinforcements in the form of fibres, whiskers, or particles. Among the various MMCs, the aluminium MMCs are prominently used in automobile and aerospace applications due to their high specific strength, wear resistance, stiffness, and corrosion resistance. In addition, reinforced MMC exhibits high tensile strength and elastic moduli compared to unreinforced metal alloys (Prathap Singh et al., 2020).

Slurry erosion has become the major failure phenomenon in turbine blades, pump impellers, valves, and pipes used in oil field equipment and power plants. Metal alloys are found to be less resistant to slurry erosion and are being replaced by MMCs in slurry handling applications. However, more work must be done on the slurry erosion of aluminium MMCs. Researchers Chand and Chandrasekhar (2020), Yadav et al. (2022), have reported the erosion behaviour under air jet erosion conditions. Furthermore, it is significant to investigate the erosion behaviour of MMCs under slurry environments.

Nguyen et al. (2014) performed the slurry erosion test on AISI 304 stainless steels by varying the testing time and impact velocity. The stainless-steel shows ductile wear behaviour and the erosion mechanism changes from the cutting, and ploughing to plastic deformation (indentation) when the angles change from oblique to normal impact angles. The authors also studied the profiles of the eroded surface and observed a ‘W’ shaped scar on the surface. The erosion was reported to be maximum at the outer surface of the scar than at the inner region (stagnation zone) due to the back pressure or cushioning effect. The influence of slurry concentration and normal impingement angle on the erosive surface damage of pipeline steels was reported by Alam and Farhat (2018). The authors stated that the erosion mechanism also depends on the slurry concentration. At higher slurry concentrations, the material removal occurs through the removal of platelets and the removal of the hardened surface layer. Due to the increased solid concentration, the solid particle-surface interaction increases the erosion rate in carbon steels. However, at higher concentrations, micro-cutting and ploughing are observed to be the secondary erosion mechanism because of the cushioning effect. The erodent properties, like hardness, shape, and size determine the wear loss and erosion mechanism. The research work of Lindgren et al. (2014) showed that the erodent properties significantly influence the wear loss of the titanium and AISI 316 stainless steel. They observed that the erosion/wear loss is not solely dependent on the impinging particle’s kinetic energy but was also influenced by the particle shape. The various equipment used for the assessment of slurry erosion is reported in the review article of Annamalai and Anand Ronald (2023).

Fang et al. (1997) investigated the slurry erosion wear behaviour of alumina fibre and in-situ TiB_2 particles reinforced aluminium MMC. They have reported that erosion behaviour depends on matrix and ceramic reinforcement material’s bonding strength and mechanical properties. Furthermore, cutting and ploughing are found to be the material removal mechanism and maximum material removal occurred at a 45° impact angle. Kumar et al. (2020) synthesised and investigated the air jet erosion behaviour of aluminium-based in situ composites with alumina abrasive particles. The authors identified craters, ductile fractures, indentation, abrasive fragments, scratches, and wear debris on the worn surface. The increase in reinforcement content reduced the erosion rate by the dispersion strengthening of reinforcement in the Al matrix. The stir-cast A356 Al-SiC composites were subjected to an erosion test at room temperature, and the authors (Saravanan et al., 1997) found that the erosion wear behaviour of the composites was mainly affected by the bond between the matrix and reinforcement and the erodent particle size. Additionally, Plastic deformation, cutting, and gouging are the main erosion mechanisms.

Chand and Chandrasekhar (2020) investigated the effect of B_4C/BN addition on the erosion behaviour of Al 6061 MMCs by considering the reinforcement content, discharge rate, erodent velocity, and impact angle as the test parameters. The authors concluded that the material erosion increases the surface roughness at a high impact angle. Furthermore, the authors found that the reduction in the wear loss was due to the increase in surface hardness due to the higher erodent discharge rate. Yadav et al. (2022) developed Al-Al_2O_3 and Al-ZrO_2 composites and performed an erosion test to assess the effect of impingement angle and impingement velocity. They reported that the reinforcement addition significantly improved the micro-hardness of the composites. Concerning the reinforcement content, the composites exhibited a range of wear mechanisms: ductile erosion, semi-ductile erosion, and semi-brittle erosion (Han et al., 2021). Vineet and Vikas (2018) have examined the erosion behaviour of surface composites produced on

ASTM A36 steel. The results showed that the WC-12%Co composite coating exhibited ductile erosion, and the Cr_3C_2–25%NiCr coating showed brittle erosion behaviour. According to Yi et al. (2016) the WC – Co composite coatings on aluminium imparted better resistance to erosion. The erosive wear of polymer matrix composites was also studied by researchers (Khan et al., 2019; Ajith et al., 2020).

From the literature, it is seen that many studies have been done on the slurry erosion behaviour of metallic materials. Researchers have also studied the wear behaviour of Al MMCs under air jet conditions with different operating parameters such as particle size and shape, erodent concentration, impact velocity, and impact angle. Moreover, the slurry erosion wear of MMCs is different from other metal alloys since the metal removal mechanism lies between ductile and brittle materials. However, no detailed investigation was found on the influence of parameters on the slurry erosive wear behaviour of Al 2124 MMCs. Materials behave differently under various operating parameters. Therefore, it is important to investigate how operating conditions influence the erosive wear behaviour of SiC reinforced Al 2124 composites.

This work focuses on investigating the slurry erosive wear behaviour of SiC-reinforced Al 2124 alloy composites with the slurry containing quartz particles with 20 g/L concentration. The influence of impingement angle and impact velocity on the composite surface was investigated. The average surface roughness and micro-hardness of the surfaces before and after erosion were examined. The microstructural analysis of eroded surfaces was performed in order to understand the material removal mechanisms.

2 Materials and methods

2.1 Composite preparation

The 2xxx series alloys have been employed in automobiles, aerospace, and structural applications owing to their excellent mechanical properties. In this study, the Al 2124 alloy has been chosen as the matrix material, and the wt.% of constituents of the alloy is shown in Table 1. In addition, 50 μm size SiC particles are selected as reinforcement. The SiC has a hardness of 9.5 (Mohs scale) and a density of 3210 kg/m^3. The composite was synthesised through the powder metallurgy (PM) technique. The metered quantity of Aluminium 2124 alloy and SiC were taken and mixed to obtain the uniform dispersion of SiC particles and to prevent the SiC cluster formation. The blended powder was filled in a die after it was cleaned using acetone to remove the impurities. Then the compaction was done at room temperature using a universal testing machine and the compacted green samples were then sintered in the furnace at 550°C for three hours. The optical micrograph of the Al matrix SiC reinforced composite is shown in Figure 1(a) and the EDS analysis of the Al – SiC composite is depicted in Figure 1(b). The micrograph confirms the reasonably uniform dispersion of SiC particles in the Al 2124 matrix.

Table 1 Wt.% of constituents in an Al 2124 alloy

Element	*Si*	*Mn*	*Zn*	*Fe*	*Mg*	*Cu*	*Al*
Wt.%	0.2	0.9	0.25	0.2	1.2–1.8	3.8–4.9	Remaining (91.2–94.7)

Figure 1 (a) Optical microscopic image of Al 2124 – SiC composite at 100X magnification and (b) EDS analysis of the Al 2124 – SiC composite (see online version for colours)

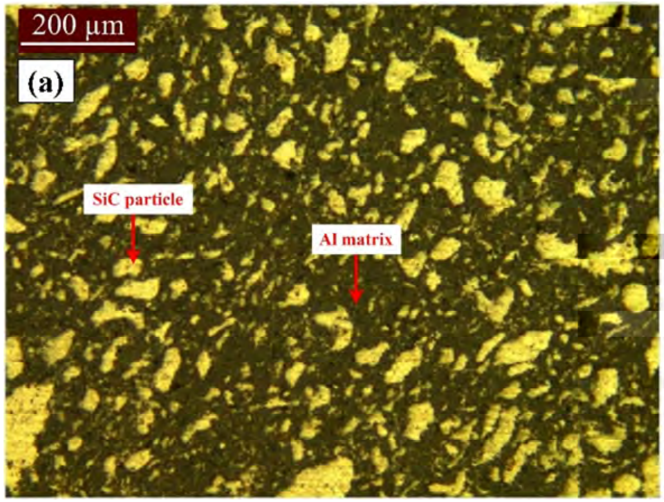

(a)

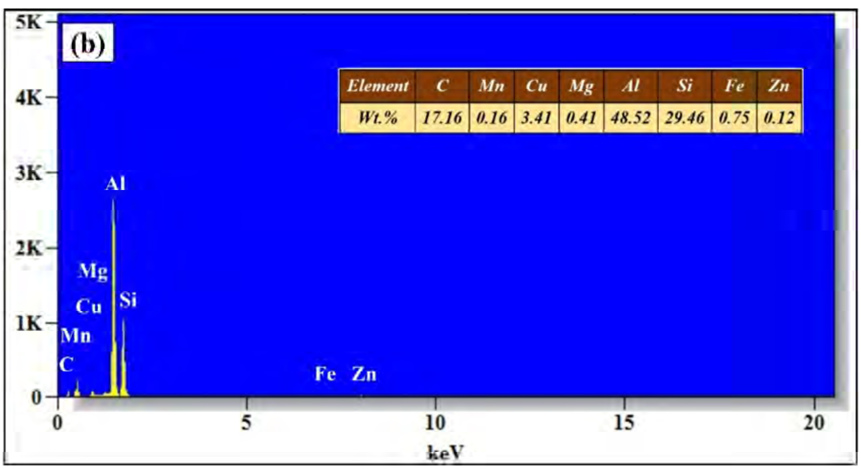

(b)

2.2 Erodent material

The quartz material was chosen as an erodent since it is naturally occurring and can be entrained in hydraulic flow applications. Quartz contains silicon dioxide and a traceable amount of impurities. Quartz has a hardness of 7 (Mohs scale) and a density of 2,650 kg/m^3. The slurry was prepared by mixing 313 µm size quartz particles with tap water. The constant 20 g/L concentration was used in this study. Figures 2(a) display the quartz particle size and shape and the particle size distribution is depicted in Figure 2(b). The various elements present in the quartz particles can be seen in Figure 2(c).

Figure 2 (a) Quartz sand particle shape, (b) particle size distribution, and (c) EDS of quartz sand (see online version for colours)

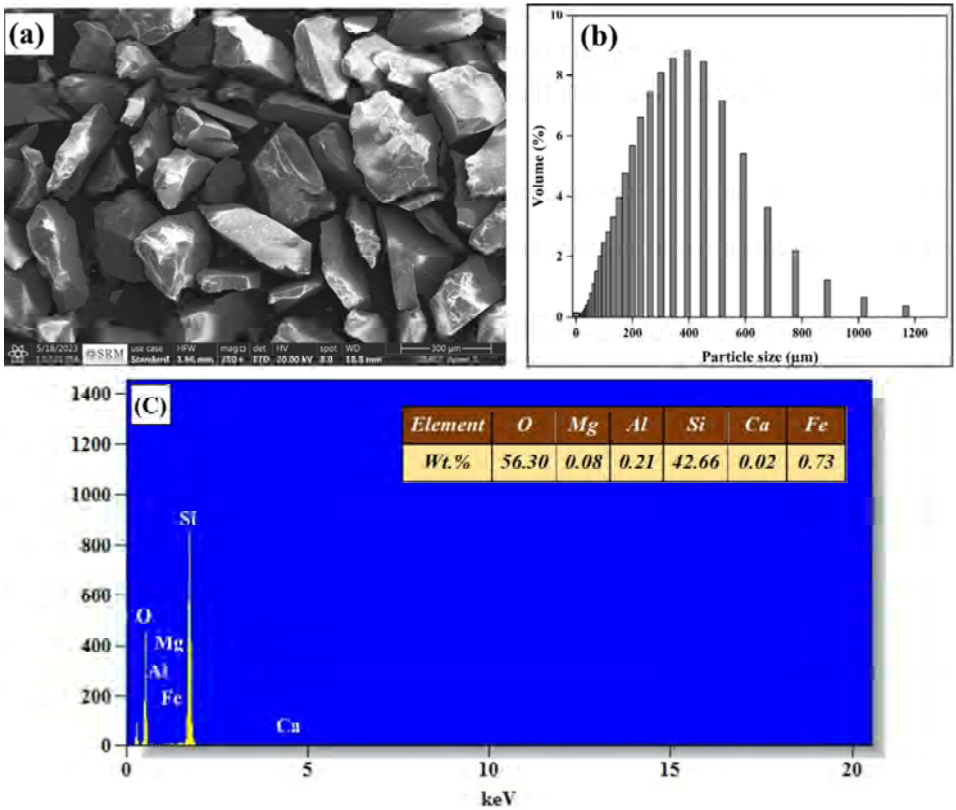

2.3 *Slurry erosion test*

The slurry erosion of aluminium-MMCs has been performed in the slurry jet impingement apparatus. The schematic diagram of the slurry jet setup is illustrated in Figure 3. This apparatus has a slurry tank in which the erodent particle-laden slurry is kept and the centrifugal pump is used to circulate the slurry. The specimen holder can be adjusted from 0°–90°. The specimen is tilted to the required angle and the slurry is impinged by the nozzle kept at the required stand-off distance. The slurry velocity can be changed by changing the flow rate since the flow rate and impact velocity are related. In this test, the mass loss occurred by impinging the hard particle-laden slurry on the target surface. The samples were polished with SiC sandpapers ranging from 80 to 2,500 mesh size. The average roughness of the polished surfaces was maintained at approximately 0.25 µm. Polished samples of size 60 × 15 × 10 mm were mounted on the angle adjustable sample holder inside the impinging area. The quartz particle concentration in the slurry was kept at 20 g/L. Each sample was exposed to the impingement of the slurry for 4 hours. The 15 mm stand-off distance was maintained for all the tests. The slurry erosion parameters are listed in Table 2. Figure 4 shows the wear profiles of the eroded samples after the slurry erosion test.

Figure 3 Illustration of the jet-type impingement erosion apparatus

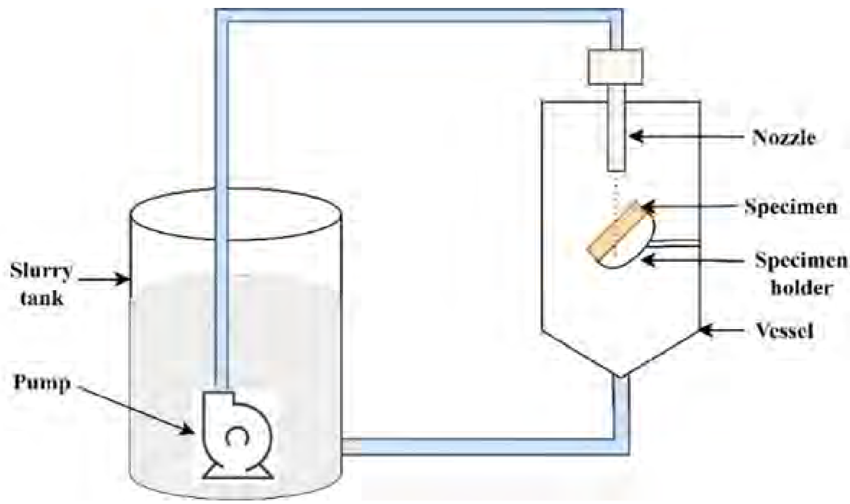

Table 2 Slurry erosion test parameters

Process parameters	*Values*
Hardness of Al 2124 – SiC composite	135 HVN_{300g}
Hardness of erodent	7 Mohs scale
Erodent size	313 µm
Erodent shape	Irregular
Erodent concentration	20 g/L
Impingement angle	45°, 60°, 75°, and 90°
Impact velocity	10, 20, and 30 m/s
Flow liquid	Water
Nozzle diameter	6 mm
Stand-off distance	15 mm
Test duration	4 hours

2.4 *Characterisation of specimens*

The eroded samples are cleaned using acetone and dried before being weighed. The wear measurement has been made in terms of mass loss in mg. The material removal mechanisms and microstructure of eroded surfaces were characterised by the scanning electron microscope. The phase transformations and erodent inclusions on the worn surface were determined by an X-ray diffractometer. The change in average surface roughness (ΔR_a) of the composite surface, before and after erosion, was measured using the surface roughness meter.

Figure 4 Wear profiles of eroded samples (see online version for colours)

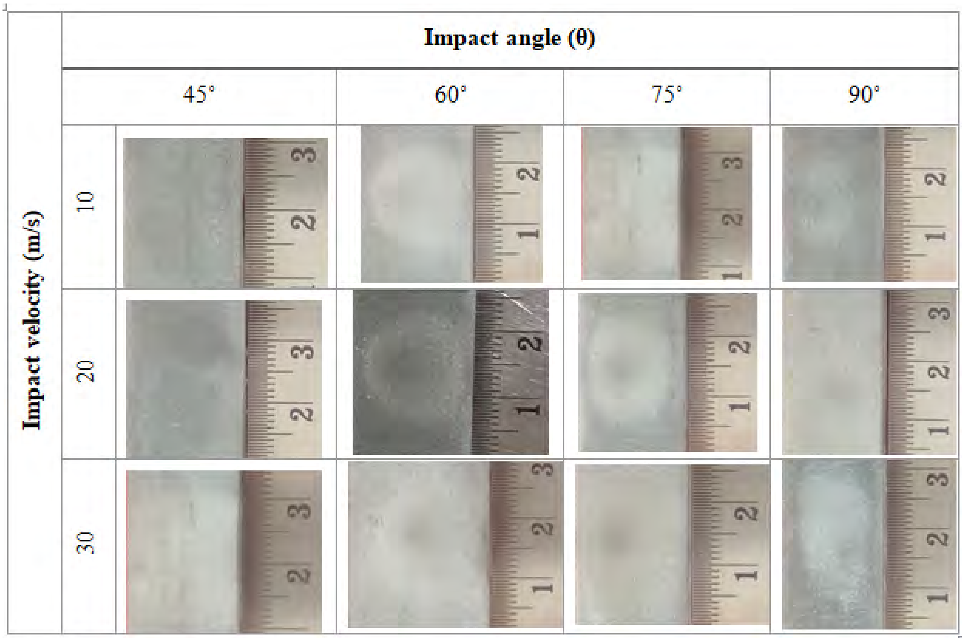

3 Result and discussion

3.1 *Effect of impingement angle on mass loss*

Mass loss was measured before and after each test using a 0.1 mg accuracy weighing machine. The angle of impingement is considered an important parameter affecting composite materials' erosion behaviour and has been thoroughly examined. Moreover, the impact velocity also influences the mass loss of the MMCs. To assess the influence of impingement angle and velocity on aluminium MMC, erosion tests were performed under the conditions mentioned in Table 1. The acute impingement angles make an elliptical wear profile on the surface, whereas the normal angle makes the circular profile illustrated in Figure 4.

In view of the results of the mass loss, it has been concluded that the slurry erosion of Al MMC is maximum at the 60° impingement angle, while is minimum at the 90° impingement angle. Moreover, the ductile nature of matrix material and the erosion mechanism varies with the impingement angle (Burstein and Sasaki 2000; López et al., 2005; Okonkwo et al., 2016). At the oblique impact angle of 45˚, the quartz-entrained slurry impinges the composite surface. The horizontal force component is much higher than the normal force, that is responsible for the scratching or ploughing of the surface causing less mass loss until the erodent passes over the surface. From Figure 12 it has been seen that the slurry erosion exhibits the extruded lips on either side of the groove. Further, due to the low normal stress at the 45° impingement angle, the mass loss due to the plastic deformation is minimum. It has been found that at a 45° impact angle, material removal by the micro-cutting mechanism seems to be lower.

Figure 5 Total mass loss as a function of impact angle at three different flow velocities with a concentration of 20 g/L of slurry and a 4-hour exposure time

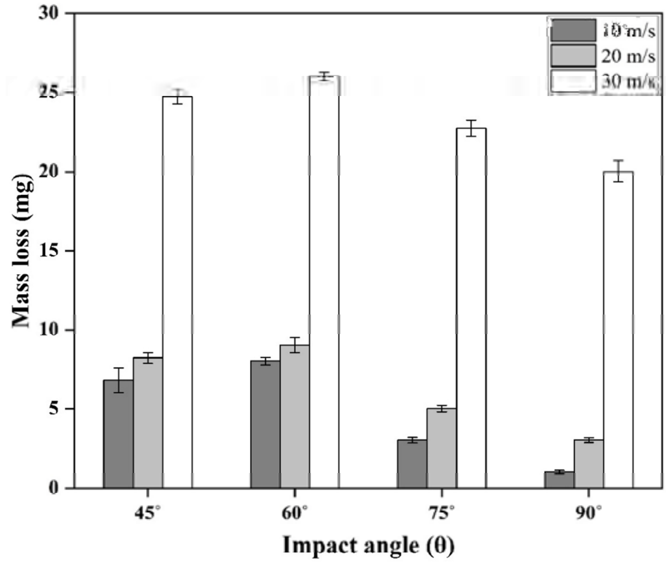

The maximum mass loss was reported at the 60° impingement angle due to the synergism between the vertical and horizontal force components as can be seen in Figure 5. The vertical force or normal stress impinges the erodent into the target surface and the horizontal force or shear stress cuts the extruded lips. In fact, slurry erosive wear is maximum on the surface of the composite at 60° impingement angle. Further increase in impingement angle caused the reduction in shear stress and increase in normal stress. The slurry erosive mechanism becomes plastic deformation, and the eroded surface appears to have shallow and deep indentations with short and thick piled-up lips all around the indentations. Meanwhile, at the 90° impact angle, the normal stress is maximum, and the shear stress is zero. Due to the minimum shear stress, the deformed extruded lips caused by the subsequent impact of erodent particles were not able to remove efficiently. Therefore, the mass loss decreases gradually with increasing impingement angles from 60° to 90° as illustrated in Figure 5.

3.2 Effect of impact velocity on mass loss

In this work three impact velocities, 10, 20, and 30 m/s were considered, and the experiments were conducted at 45°, 60°, 75°, and 90° impingement angles. The variation of mass loss as a function of velocity is displayed in Figure 6. It is obvious that an increase in velocity increases the mass loss in all conditions. For instance, in Figure 6, the maximum mass loss was observed at 30 m/s impact velocity and 60° impact angle. In all the impact angles, the maximum mass loss occurred at the 30 m/s impact velocity. Furthermore, the increase in mass loss is expected as the higher particle velocity increases the kinetic energy with which the particle hits the target surface, thereby increasing the mass loss. The mathematical model developed by Finnie (1960, 1972) stated that the volume of material removal is proportional to the square of the particle velocity. Hutchings (1981) demonstrated that the erosion ratio is proportional to the n^{th} power of the particle velocity.

Figure 6 Total mass loss as a function of flow velocity at four impact angles with a concentration of 20 g/L of slurry and an exposure time of 4 hours

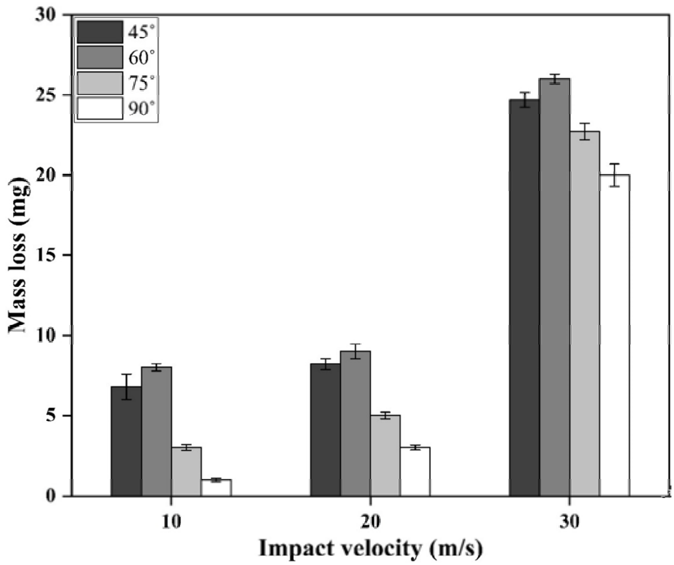

It is seen that the rapid increase in mass loss was observed from 20 m/s to 30 m/s. According to the Hutchings erosion model (Hutchings, 1981), the loss of material occurred in two ways:

1 When the plastic strain of the extruded lips reaches the critical value

2 Due to the low cycle fatigue by the subsequent impingement of particles with high kinetic energy imparted by higher erodent velocity.

Meanwhile, at 30 m/s impact velocity, the increased straining or deformation results in higher mass loss. Though the particle velocity increases the mass loss, it also depends on other parameters such as impact angle, particle shape, particle hardness, particle concentration, and target material properties. From Figure 6, it has been observed that at 30 m/s impact velocity, 90° impact angle yielded minimum mass loss due to the minimum shear stress. However, irrespective of impact velocity, the mass loss was maximum at 45°–60° impact angles. From the SEM images (Figure 12), it is clear that at 30 m/s flow velocity, the particle pull-out due to the erosion of nearby soft matrix, micro-cutting, and crater formation is rampant, which in turn causes excessive mass loss. The erodent particles impinge on the target material and take away the material by microchips or leave the extruded lip on the surface.

The recent research work of Chouhan et al. (2023) has investigated the slurry erosion behaviour of tantalum by considering impact angle, impact velocity, and solid concentration as the test parameters. As predicted, the erosion rate increased linearly with an increase in impact velocity at shallow and normal impact angles.

3.3 Surface roughness analysis

The average surface roughness (R_a) of the MMC surface before and after the test was measured to establish the relationship between the roughness and test parameters: impact angle and impact velocity. The average roughness measurement (R_a) was made using the roughness tester (Model: Mitutoyo SJ-210) with a cut-off length of 0.8 mm and a total evaluation length of 4 mm. The surface roughness measurements were performed thrice and the average values are used to present the data. The surface of the target material experienced roughness changes during the slurry erosion and resulting in a rougher surface (Elemuren et al., 2019; Wang and Zheng 2021). Figures 7 and 8 illustrate the influence of impact angle and flow velocity on the change in surface roughness (ΔR_a) of the sample surface before and after the impingement. ΔR_a for the impact angles (45°, 60°, and 90°) does not show any significant variation. A slight decrease in ΔR_a was reported at an impact angle of 60° and 10 m/s flow velocity. The high mass loss occurred due to the fatigue of the extruded lips, and the complete removal of the material makes the surface comparatively smoother at 45˚ than 90˚ impact angles. It has been found that the flow velocity greatly influences the ΔR_a. The particle with high kinetic energy tends to deform or erode the surface plastically. Therefore, in all flow velocities, ΔR_a is increased. The maximum ΔR_a was reported at a 45° impact angle with 30 m/s flow velocity. The material loss would be maximum when the velocity of flow reaches beyond the threshold, i.e., critical flow velocity (CFV). Yi et al. (2021) have investigated the CFV for erosion-corrosion of SS304 by means of surface roughness. Similarly, in another research work, Yi et al. (2018) determined CFV for six grades of stainless-steel using surface roughness as an indicator. Furthermore, the changes in the surface roughness related with the mass loss, and hence, roughness measurement can also be used as an indicator of CFV.

Figure 7 Surface roughness gradient (ΔR_a) of Al MMC samples as a function of impact angle after impingement by slurry with 20 g/L quartz particles for 4 hours of exposure

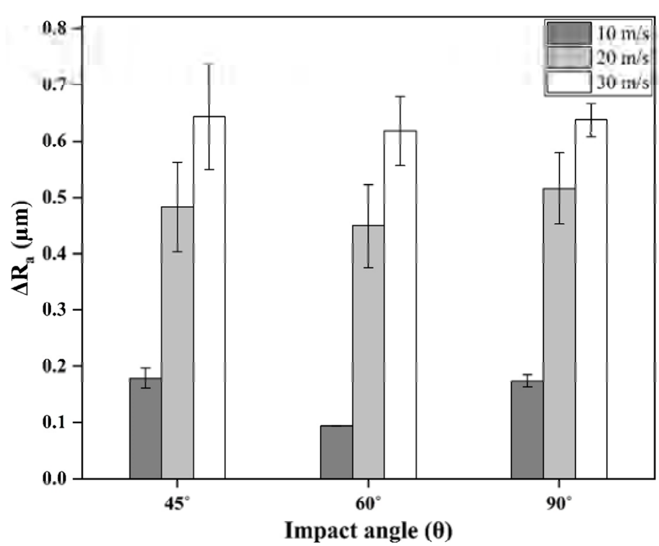

Figure 8 Surface roughness gradient (ΔR_a) of Al MMC samples as a function of impact velocities after impingement by slurry with 20 g/L quartz particles for 4 hours of exposure

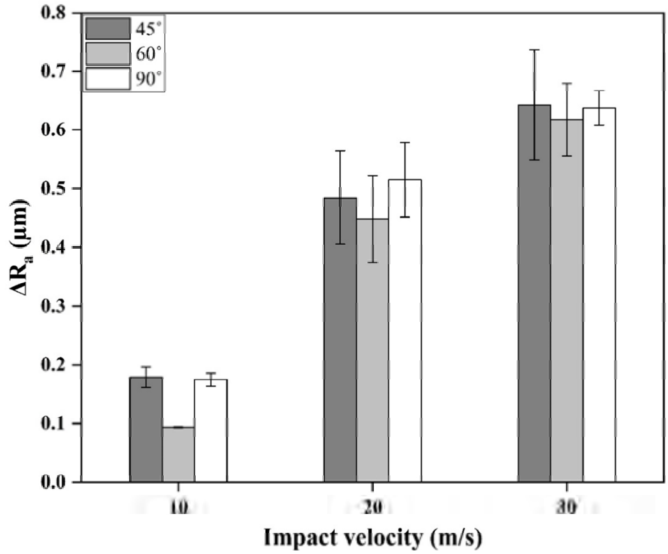

3.4 Hardness profile of the eroded surface

The hardness is the surface property that shows how resistant a surface is against penetration. The increased hardness of the eroded surface is an evident of strain hardening by high energy particle impact (Aribo et al., 2013). Venkatraman Krishnan and Lim (2021), have investigated the slurry erosion behaviour of S275JR steel and stated that the surface hardness of the target material increased, and the hardness decreased as the depth increased. The increase in hardness is evident that the grains along the surface were strained due to the impingement of high kinetic energy particles over the surface. The research work of Aribo et al. (2013), has witnessed the eroded surface with increased micro-hardness due to the strain hardening. The micro-hardness profile of the eroded surface of the Al 2124 matrix SiC-reinforced composite samples at 20 m/s and 30 m/s impact velocity and 60° and 90° impact angles with 20 g/L quartz sand concentration for 4-hour test duration was shown in Figure 9. The micro-hardness profile on the eroded surface shows an inconsistent hardness value. Since the composite contains 5 wt.% of SiC hard particles, the uneven micro-hardness values resulted from the eroded surface, which has strain-hardened matrix and exposed hard reinforcement particles, as seen in Figure 12. Figures 12, 13 and 14 showed that the reinforcement particles were exposed due to the erosion of the soft matrix around particles caused the protrusion over the composite surface resulting in the maximum hardness value. The decline in the hardness value is due to either indentation over a soft matrix or the reinforcement particles being completely pulled out along the craters, which left only the matrix material.

Figure 9 Micro-hardness profile of the cross-section (A–A) of composites after erosion by quartz in tap water at 20 and 30 m/s impact velocity and 60° and 90° impact angle for 4 hours exposure time (see online version for colours)

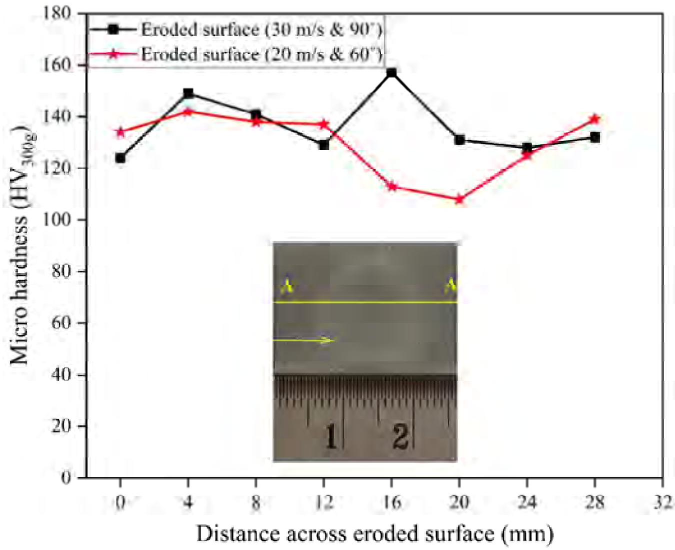

Note: Arrow showing the direction the hardness was taken.

Figure 10 XRD patterns of Al 2124 + SiC composite specimen before and after erosion at 30 m/s flow velocity and 90° impact angle for 4-hour slurry exposure (see online version for colours)

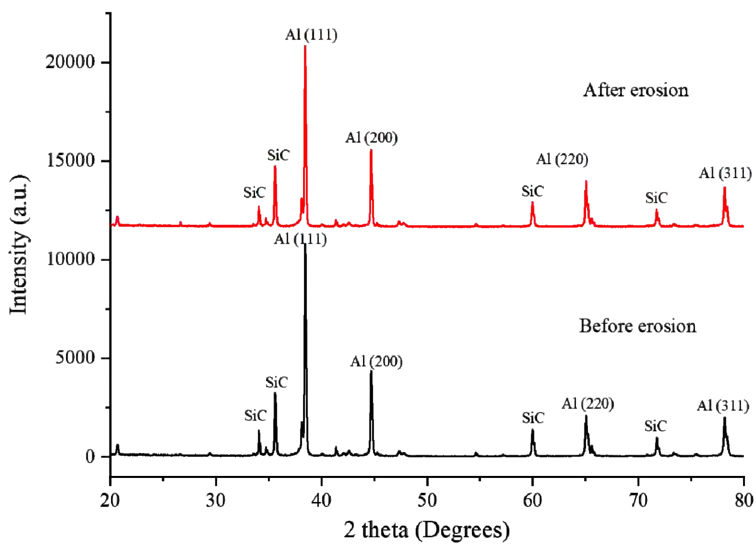

3.5 X-ray diffraction (XRD) studies

XRD studies were done on the samples after cleaning them with acetone. XRD was done on the polished and eroded surface to find the possible inclusions and phase transformations of the eroded surface due to the prolonged exposure of the samples in a slurry environment. Figure 10 displays the XRD pattern of the composite specimen before and after erosion at 30 m/s flow velocity, 90° impact angle, and 20 g/L quartz particle concentration for the 4-hour test duration. From the XRD pattern, it has been concluded that no particle inclusion and phase transformation was found on the worn surface. Due to surface erosion, the Al peak (111) has been reduced compared to the polished surface, as seen in Figure 10. Aribo et al. (2013) observed that the reduction in the peak was attributed to the strain hardening of the eroded surface.

3.6 Erosion mechanisms

Erosion is a progressive loss of material due to the interaction of solid particles, liquid impingement, cavitation, and liquid-solid two-phase flow. The mass loss is different in each erosion type. In slurry erosion, mass loss occurs by the impingement of solid particles of high kinetic energy imparted by the fluid flow. Cutting, ploughing, and indentation was the majorly found material removal mechanisms in the metals (Annamalai and Anand Ronald, 2023). The SEM analysis of the eroded samples was done to interpret the underlying mechanisms of erosion. Unlike metals, the composite behaves differently when subjected to an erosion test. The ductile materials exhibited higher mass loss at the shallow impingement angle, and the brittle material showed higher mass loss at the normal impingement angle. However, the material loss in the brittle material occurs by fracturing the target surface. In ductile materials, removal occurs by cutting or platelets developed by ploughing and the subsequent removal of platelets. The metal removal mechanism of MMCs lies between the ductile matrix and the brittle reinforcement material (Han et al., 2021).

The research work of Fang et al. (1999) disseminated an interesting phenomenon called the ‘shadowing effect’ which is responsible for the improved erosion resistance of composite at oblique angles. They developed a SiC-reinforced titanium matrix composite and tested it with slurry erosion. The maximum erosion was observed at 15°–30° and 90° for ductile matrix and hard reinforcement respectively. However, SiC-reinforced titanium composite exhibited maximum erosion at a 45° impact angle. The effect of reducing the impact energy exerted by the SiC erodent on SiC fibre at a higher attacking angle. At the low-angle impact, the titanium matrix was protected by the shadowing effect of SiC reinforcement. In accordance with the previous research (Fang et al., 1999; Acharya et al., 2008; Ramesh and Keshavamurthy, 2011), the maximum mass loss observed at low impact angles say 15°–30°. However, in the present study, the maximum mass loss was observed at a 60° impact angle. This is due to the shadow effect reported by Fang et al. (1999). At low-impact angles, the kinetic energy exerted by the erodent particles was absorbed by SiC reinforcements. Hence, the hard SiC particles in the Al 2124 composite improved the erosion resistance at shallow impact angles. Further, the soft Al matrix is susceptible to low-angle erosion, since at a low-impact angle the shear stress is maximum which will accelerate the material removal by cutting and ploughing. The SiC reinforcements act as a barrier and prevent the cutting and ploughing up to a certain extent to enhance erosion resistance.

Micro-cutting, ploughing, indentation, spalling, scouring, gouging, pulling out of fibres and particles and fracturing were the mechanisms of material removal in composites as reported by the researchers (Grewal et al., 2013; Nithin et al., 2018; Chen et al., 2020). The erosion mechanisms in materials can be related to cutting, ploughing, and indentation, as seen in Figure 11. For ductile material, mass loss mechanism varies at both oblique and normal impact angles. At the oblique impact angle (5°–25°), the ductile materials exhibit cutting (see Figure 11(a)) since the particle has the sufficient shear component to detach the material from the surface. On the other hand, when the oblique angle increases to 25°–85°, due to the decrease in shear component the impinging particle is able to displace the material from the surface and not completely detach from the surface as seen in Figure 11(c). The displaced material piles up or forms extruded lips along the edges of the groove and the material removal occurs by the subsequent impact that causes the large plastic strain on the lips. Figure 11(d) shows the cracks on the extruded lips formed by the continued impingement of erodent. When the erodent particle impinges the material surface at 90°, there is no horizontal component of velocity, consequently, the impinging particle exerts zero shear stress on the material surface. Therefore, the kinetic energy imparted by the erodent to the target material was absorbed as the strain energy resulting in an indentation with the displaced material on all sides of the erodent as shown in Figure 11.

Figure 11 The diagram shows the material removal (mass loss) mechanisms, (a) cutting, (b) indentation, (c) and (d) ploughing (see online version for colours)

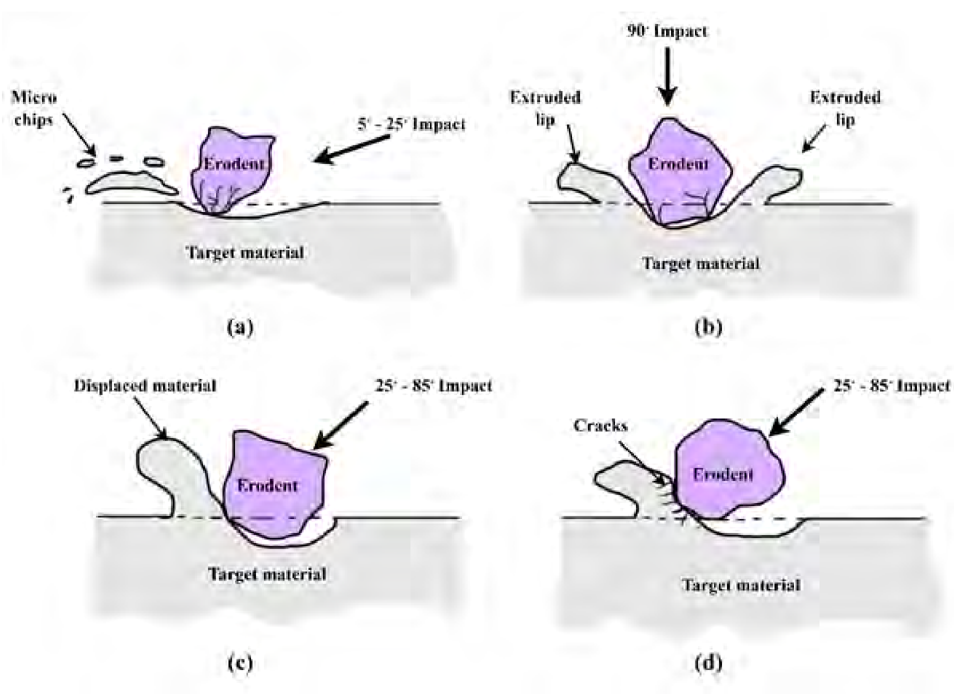

The erosion mechanism changes concerning the impingement angle. The SEM images of 60°, 75°, and 90° impact angles are shown in Figures 12, 13 and 14, respectively. The Al 2124 matrix SiC-reinforced composite surface was exposed to the slurry jet at a flow velocity of 30 m/s and an impact angle of 60° for a test duration of 4 hours as shown in Figure 12. The exposed SiC particles and grooves on the eroded surface show that particle pull-out and ploughing could be the dominant material removal mechanism. Micro-cutting was also found to be the material removal mechanism. In the erosion testing of tantalum, Chouhan et al. (2023) found that erosion was purely plastic deformation induced by impinging particles. The authors have reported a negative erosion rate i.e., mass gain after the erosion test. During the erosion, a few broken erodent particles were embedded on the severely strained surface. In the present study, for all the experiments mass loss was observed and the XRD analysis of the eroded samples also confirm that there was no quartz embedment on the surface.

Figure 12 SEM image shows the eroded surface of a composite tested with 30 m/s impact velocity and 60° impingement angle for 4 hours of slurry impingement (see online version for colours)

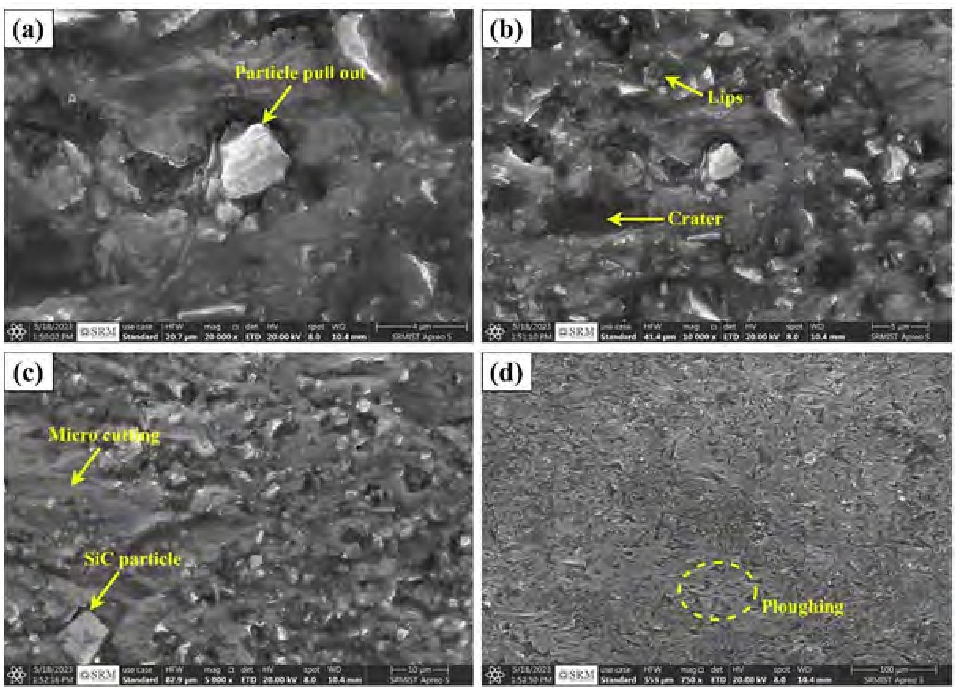

In most cases, the mixed micro-cutting and ploughing were responsible for the metal removal rather than the pure cutting and ploughing. Figures 12(c) and 12(d) show the extruded lips formed due to acute-angle ploughing since the erodent particle impinges the target surface and plastically deformed material that tends to flow outward and accumulate on either side of the grooves. The subsequent impingements remove the platelets due to fatigue, making the surface less rough. There is a reduction in wear loss at the lower impingement angle and impact velocity as the solid particle strikes the surface and slides over the target surface, inducing fatigue fracture and strain hardening (Chand and Chandrasekhar, 2020). The induced energy by the striking erodent particles is responsible for the plastic deformation of the surface (Alam and Farhat, 2018). Indentation and reinforcement pull-out can also be observed on the eroded surface. The pull-out of SiC from the eroded surface indicates that the matrix material does not have sufficient binding strength to hinder the pull-out of reinforcement from the surrounding matrix material. Due to this, the plastic deformation of the ductile matrix material increases, giving rise to the total mass loss. The exposed reinforcement particles and craters can be observed in Figure 12(a).

Figure 13 The SEM image shows the eroded surface of a composite tested with an impact velocity of 30 m/s and an impingement angle of 75° for 4 hours of impingement of the slurry

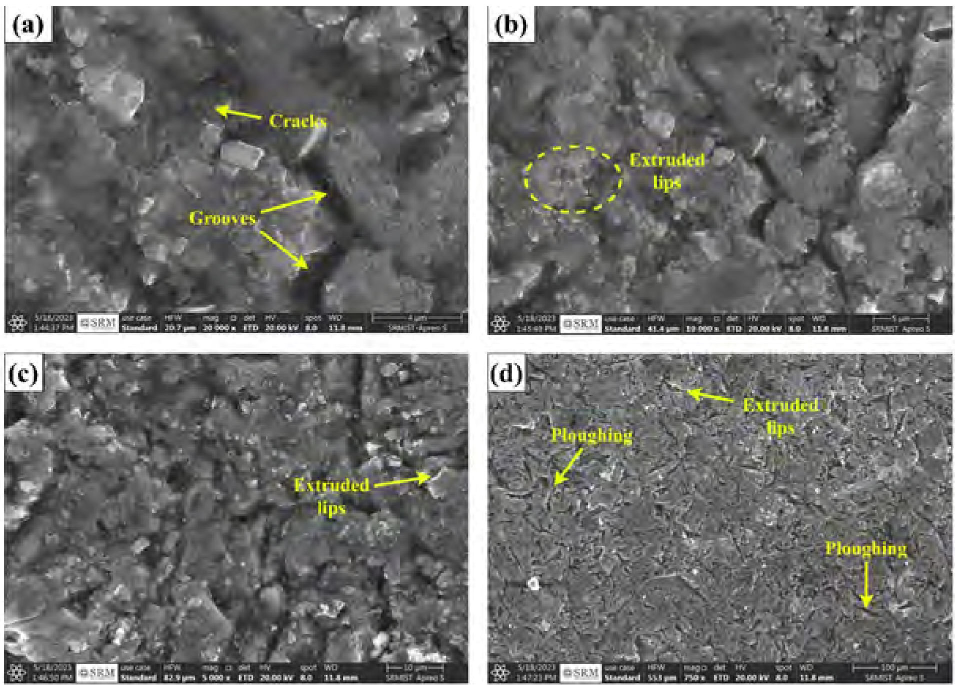

The shallow impact angle has been found to cause micro-cutting and ploughing. However, the high impact angle on the normal incidence of the particle leads to indentation and craters. Figure 12(d) shows the grooves in the direction of the impact as a result of the impact angle of 60°. The grooves become random and shallow as the impingement angle changes to 90°. At a normal impingement angle, the indentation becomes the major material removal mechanism due to the vertical component of force. The material removal mechanism can be interpreted by the normal and shear stress imparted by the impinging particle on the target surface. At lower impact angles, the shear stress becomes high, pushing the material in the direction of ejection to cause a scratch or plough mark on the surface. The continuous impingement of particles on the displaced material along the grooves dislodges the material in the form of chips, which in turn causes severe wear loss. It was also observed that the increase in impact angle weakens the shear force responsible for the material removal. Due to this, the grooves appeared to be random and shallow, resulting in reduced wear loss. At a normal impact angle, the normal stress is higher, plastically deforms the surface, and indentation and craters are observed (Zhao et al., 2015).

Figure 14 SEM micrograph of the eroded surface of a composite at 30 m/s impact velocity and 90° impingement angle after 4 hours of slurry impingement (see online version for colours)

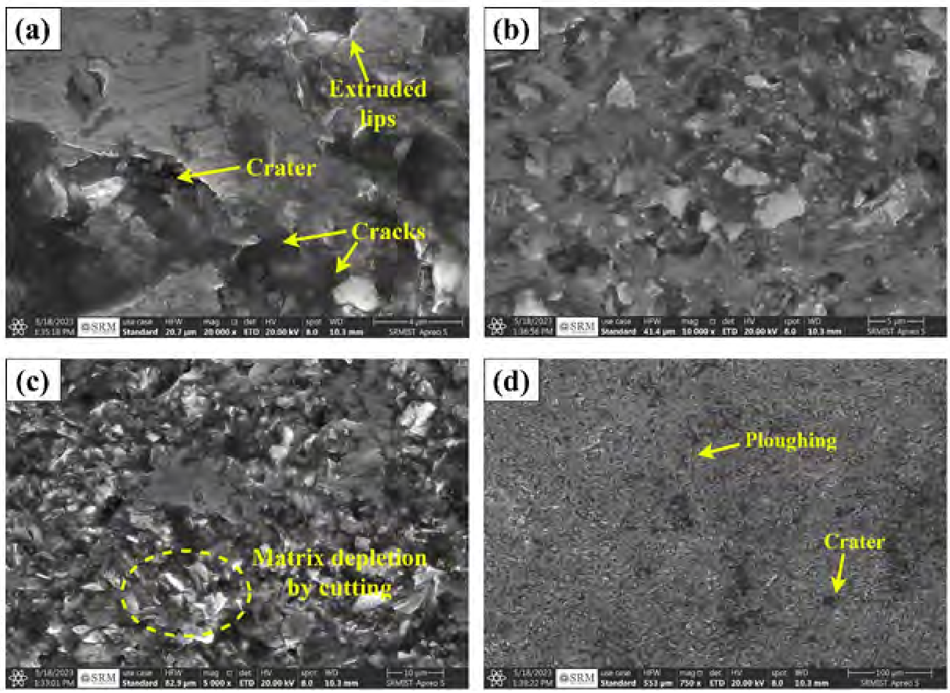

Figure 13 displays the eroded surface of AMC at 30 m/s impact velocity and 75° impingement angle after 4 hours of slurry impingement. At a 75° impact angle, the lips and exposed SiC particles can be seen on the eroded surface due to the impact of erodent particles. Initially, the material removal occurred on the matrix material, and the regions where the depleted Al matrix can be seen in Figures 13 and 14 because of the increased impact velocity of 30 m/s. Craters, shallow grooves, and particle pull-out were found on the eroded surface of the composite at a 90° angle and 30 m/s velocity. Furthermore, the platelet mechanism dominated material removal at a 90° impact angle. Cracks on the eroded surface can be seen in Figure 14(a). Many researchers have found that the reinforcement fracturing on the eroded surface of the composite (Grewal et al., 2013; Sharma et al., 2019; Panwar et al., 2020). However, in this study reinforcement fracturing is not observed since we used the quartz particle as the erodent which has less hardness than the SiC particle. Moreover, particle pull-out due to the erosion of the aluminium matrix, ploughing, and cutting were observed to be the major material removal mechanisms.

4 Conclusions

The slurry erosive behaviour of the Al 2124 matrix composite fabricated by the PM process has been studied concerning different conditions. The results of this study are given as follows:

1 The mass loss of the composite specimens increases with an increase in impact velocity. This is due to the high kinetic energy of the impinging particles imparted by the flow velocity. Maximum mass loss was reported at 30 m/s impact velocity.

2 Impingement angle also influences the erosion mechanism. From the test results, it has been seen that mass loss is higher for 45°–60° than 75°–90° impact angle. At lower impingement angles, the shear force component is higher, which can push the material to cause scratches or grooves on the target surface.

3 The XRD pattern of the specimens before and after the erosion test reveals no erodent inclusion and the new phase transformation due to 4-hour slurry exposure.

4 The surface roughness examination before and after erosion confirms that increased impact velocity significantly increases roughness.

5 Micro-cutting, ploughing, particle pull-out, and craters are found to be material removal mechanisms. At 60° impact angle, ploughing and cutting dominated the material removal, whereas, at 90° impact angle, the platelet mechanism and crater were responsible for the material removal. Matrix-depleted regions were observed on the eroded surface at normal impingement angles.

Acknowledgements

The authors thank SSN Trust for the financial support (Grant No: SSN/IFFP/DECEMBER 2021/1-21/06) to carry out this research under the Internally funded faculty project 2021-22.

References

Acharya, S.K., Dikshit, V. and Mishra, P. (2008) 'Erosive wear behaviour of redmud filled metal matrix composite', *J. Reinf. Plast. Compos.*, Vol. 27, No. 2, pp.145–152, DOI: 10.1177/0731684407082543.

Ajith, G., Joshi, P., Kumar, M. and Basavarajappa, S. (2020) 'Investigation on slurry erosion of Al_2O_3 incorporated glass/epoxy composites', *Int. J. Surf. Sci. Eng.*, Vol. 14, No. 4, pp.257–273, DOI: 10.1504/IJSURFSE.2020.112277.

Alam, T. and Farhat, Z.N. (2018) 'Slurry erosion surface damage under normal impact for pipeline steels', *Eng. Fail. Anal.*, Vol. 90, pp.116–128, DOI: 10.1016/j.engfailanal.2018.03.019.

Annamalai, S. and Anand Ronald, B. (2023) 'A comprehensive review on synergistic and individual effects of erosion–corrosion in ferrous piping materials', *Corros. Rev.*, Vol. 41, No. 4, DOI: 10.1515/corrrev-2022-0063.

Aribo, S., Barker, R., Hu, X. and Neville, A. (2013) 'Erosion-corrosion behaviour of lean duplex stainless steels in 3.5% NaCl solution', *Wear*, Vol. 302, Nos. 1–2, pp.1602–1608 DOI: 10.1016/j.wear.2012.12.007.

Aribo, S., Fakorede, A., Ige, O. and Olubambi, P. (2017) 'Erosion-corrosion behaviour of aluminum alloy 6063 hybrid composite', *Wear*, Vol. 376–377, pp.608–614, DOI: 10.1016/j.wear.2017.01.034.

Burstein, G.T. and Sasaki, K. (2000) 'Effect of impact angle on the slurry erosion-corrosion of 304L stainless steel', *Wear*, Vol. 240, Nos. 1–2, pp.80–94, DOI: 10.1016/S0043-1648(00)00344-6.

Chand, S. and Chandrasekhar, P. (2020) 'Influence of B_4C/BN on solid particle erosion of Al 6061 metal matrix hybrid composites fabricated through powder metallurgy technique', *Ceram. Int.*, Vol. 46, No. 11, pp.17621–17630, DOI: 10.1016/j.ceramint.2020.04.064.

Chen, Y., Wu, Y., Hong, S., Long, W. and Ji, X. (2020) 'The effect of impingement angle on erosion wear characteristics of HVOF sprayed WC-Ni and WC-Cr_3C_2-Ni cermet composite coatings', *Mater. Res. Express*, Vol. 7, No. 2, DOI: 10.1088/2053-1591/ab6d31.

Chouhan, J.S., Jana, B.D., Purandare, Y.P., Dey, A., Hovsepian, P.E., Jenkins, D. and Jones, L. (2023) 'Preliminary investigation of slurry erosion behaviour of tantalum', *Wear*, Vols. 516–517, p.204605, DOI: 10.1016/J.WEAR.2022.204605.

Elemuren, R., Tamsaki, A., Evitts, R., Oguocha, I.N.A., Kennell, G., Gerspacher, R. and Odeshi, A. (2019) 'Erosion-corrosion of 90° AISI 1018 steel elbows in potash slurry: Effect of particle concentration on surface roughness', *Wear*, Vols. 430–431, pp.37–49, DOI: 10.1016/j.wear.2019.04.014.

Fang, Q., Sidky, P. and Hocking, M.G. (1997) 'Erosive wear behaviour of aluminium based composites', *Mater. Des.*, Vol. 18, Nos. 4–6, pp.389–393, DOI: 10.1016/S0261-3069(97)00081-2.

Fang, Q., Sidky, P.S. and Hocking, G.M. (1999) 'Erosion resistance of continuously reinforced SiC-Ti-based metal matrix composites by a SiC/water slurry jet', *Wear*, Vols. 233–235, pp.174–181, DOI: 10.1016/S0043-1648(99)00232-X.

Finnie, I. (1960) 'Erosion of surfaces by solid particles', *Wear*, Vol. 3, No. 2, pp.87–103, DOI: 10.1016/0043-1648(60)90055-7.

Finnie, I. (1972) 'Some observations on the erosion of ductile metals', *Wear*, Vol. 19, No. 1, pp.81–90, DOI: 10.1016/0043-1648(72)90444-9.

Grewal, H.S., Agrawal, A. and Singh, H. (2013) 'Slurry erosion performance of Ni-Al_2O_3 based composite coatings', *Tribol. Int.*, Vol. 66, pp.296–306, DOI: 10.1016/j.triboint.2013.06.010.

Han, X., Xu, D., Axinte, D., Liao, Z. and Li, H.N. (2021) 'On understanding the specific cutting mechanisms governing the workpiece surface integrity in metal matrix composites machining', *J. Mater. Process. Technol.*, Vol. 288, p.116875, DOI: 10.1016/J.JMATPROTEC.2020.116875.

Hutchings, I.M. (1981) 'A model for the erosion of metals by spherical particles at normal incidence', *Wear*, Vol. 70, No. 3, p.269, DOI: 10.1016/0043-1648(81)90347-1.

Ishfaq Amin, M. and Harmain, G.A. (2021) 'An assessment of erosive wear of hydro-turbine steel using statistical modelling and optimisation', *Int. J. Surf. Sci. Eng.*, Vol. 15, No. 1, pp.1–17, DOI: 10.1504/IJSURFSE.2021.10037020.

Khan, M.A., Manikandan, S., Ebenezer, G., Uthayakumar, M. and Thirumalai Kumaran, S. (2019) 'Solid particle erosion studies on fibre composite with egg shell as filler materials', *Int. J. Surf. Sci. Eng.*, Vol. 13, No. 1, pp.1–13, DOI: 10.1504/IJSURFSE.2019.097910.

Kumar, S., Manani, S., Nikunj, P. and Pradhan, A.K. (2020) 'Synthesis and air jet erosion wear behavior of aluminum – Al_3Ti In-Situ composite', *Mater. Today Proc.*, Vol. 28, pp.2572–2578, DOI: 10.1016/j.matpr.2020.05.701.

Lindgren, M. and Perolainen, J. (2014) 'Slurry pot investigation of the influence of erodant characteristics on the erosion resistance of titanium', *Wear*, Vol. 321, pp.64–69, DOI: 10.1016/j.wear.2014.10.005.

López, D., Congote, J.P., Cano, J.R., Toro, A. and Tschiptschin, A.P. (2005) 'Effect of particle velocity and impact angle on the corrosion-erosion of AISI 304 and AISI 420 stainless steels', *Wear*, Vol. 259, Nos. 1–6, pp.118–124, DOI: 10.1016/j.wear.2005.02.032.

Miyazaki, N. and Funakura, S. (1996) 'Solid particle erosion behavior of metal matrix composites', *J. Compos. Mater*, Vol. 30, No. 15, pp.1670–1682, DOI: 10.1177/002199839603001503.

Nguyen, Q.B., Lim, C.Y.H., Nguyen, V.B., Wan, Y.M., Nai, B., Zhang, Y.W. and Gupta, M. (2014) 'Slurry erosion characteristics and erosion mechanisms of stainless steel', *Tribol. Int.*, Vol. 79, pp.1–7, DOI: 10.1016/j.triboint.2014.05.014.

Nithin, H.S., Desai, V. and Ramesh, M.R. (2018) 'Elevated temperature solid particle erosion behaviour of carbide reinforced CoCrAlY composite coatings', *Mater. Res. Express*, Vol. 5, No. 6, DOI: 10.1088/2053-1591/aac998.

Okonkwo, P.C., Shakoor, R.A., Zagho, M.M. and Amer Mohamed, A.M. (2016) 'Erosion behaviour of API X100 pipeline steel at various impact angles and particle speeds', *Metals*, Vol. 6, No. 10, DOI: 10.3390/met6100232.

Panwar, V., Grover, N.K. and Chawla, V. (2020) 'Erosion studies of plasma sprayed WC-12%Co, Cr_3C_2-25%NiCr, 80%Ni-20%Cr, 87%Al_2O_3-13%TiO_2 coatings on ASTM A36 steel', *Mater. Res. Express*, Vol. 7, No. 2, DOI: 10.1088/2053-1591/ab7072.

Prathap Singh, S., Prabhuram, T., Vinoth Babu, K., Elilraja, D., Uthayakumar, M. and Rajan, T.P.D. (2020) 'Solid particle erosion studies on SiC reinforced functionally graded aluminium matrix composites', *IOP Conf. Ser.: Mater. Sci. Eng.*, Vol. 764, No. 1, DOI: 10.1088/1757-899X/764/1/012005.

Ramesh, C.S. and Keshavamurthy, R. (2011) 'Slurry erosive wear behavior of Ni-P coated Si_3N_4 reinforced Al 6061 composites', *Mater. Des.*, Vol. 32, No. 4, pp.1833–1843, DOI: 10.1016/j.matdes.2010.12.024.

Saravanan, R., Surappa, M. and Pramila Bat, B. (1997) 'Erosion of A356 Al SiC_p composites due to multiple particle impact', *Wear*, Vol. 202, No. 2, pp.154–164, DOI: 10.1016/S0043-1648(96)07264-X.

Sharma, V., Kaur, M. and Bhandari, S. (2019) 'Slurry erosion performance study of high velocity flame sprayed Ni-Al_2O_3 coating under hydro accelerated conditions', *Mater. Res. Express*, Vol. 6, No.7, DOI: 10.1088/2053-1591/ab1927.

Venkatraman Krishnan, A. and Lim, C.Y.H. (2021) 'Elucidating the specific and combined effects of particle size, impact angle, velocity and stress from an external load on the slurry erosion of mild steel S275JR', *J. Mater. Res. Technol.*, Vol. 14, pp.1052–1064, DOI: 10.1016/j.jmrt.2021.07.013.

Vineet, S. and Vikas, C. (2018) 'Solid particle erosion studies of D-gun sprayed cermet coatings on ASTM A36 steel', *Int. J. Surf. Sci. Eng.*, Vol. 12, No. 4, pp.317–335, DOI: 10.1504/IJSURFSE.2018.10017426.

Wang, Z.B. and Zheng, Y.G. (2021) 'Critical flow velocity phenomenon in erosion-corrosion of pipelines: determination methods, mechanisms and applications', *J. Pipeline Sci. Eng.*, Vol. 1, No. 1, pp.63–73, DOI: 10.1016/j.jpse.2021.01.005.

Yadav, M., Kumaraswamidhas, L.A. and Singh, S.K. (2022) 'Investigation of solid particle erosion behavior of Al-Al_2O_3 and Al-ZrO_2 metal matrix composites fabricated through powder metallurgy technique', *Tribol. Int.*, Vol. 172, DOI: 10.1016/j.triboint.2022.107636.

Yi, J., He, S., Wang, Z., Hu, H. and Zheng, Y. (2021) 'Effect of Impact Angle on the Critical Flow Velocity for Erosion–Corrosion of 304 Stainless Steel in Simulated Sand-Containing Sea Water', J. Bio- Tribo-Corros., Vol. 7, No. 3, DOI: 10.1007/s40735-021-00538-z.

Yi, J.Z., Hu, H.X., Wang, Z.B. and Zheng, Y.G. (2018) 'Comparison of critical flow velocity for erosion-corrosion of six stainless steels in 3.5 wt% NaCl solution containing 2 wt% silica sand particles', *Wear*, Vols. 416–417, pp.62–71, DOI: 10.1016/j.wear.2018.10.006.

Yi, X., Xiaohan, P. and Songbo, W. (2016) 'Investigation of erosion resistance property of WC-Co coatings', *Int. J. Surf. Sci. Eng.*, Vol. 10, No. 4, pp.365–374, DOI: 10.1504/IJSURFSE.2016.077536.

Zhao, Y., Zhou, F., Yao, J., Dong, S. and Li, N. (2015) 'Erosion-corrosion behavior and corrosion resistance of AISI 316 stainless steel in flow jet impingement', *Wear*, Vols. 328–329, pp.464–474, DOI: 10.1016/j.wear.2015.03.017.